Communication

Design of a Seven-Component Eutectic High-Entropy Alloy

M.R. RAHUL and GANDHAM PHANIKUMAR

A eutectic high-entropy alloy with seven components (Fe, Ni, Cr, V, Co, Mn, and Nb) was designed via the melt route guided by CALPHAD predictions. Configurational entropy estimated for the two-phase microstructure qualifies it to be referred to as a high-entropy alloy. When the Nb content exceeded 9.7 at. pct, the microstructure changed from hypoeutectic with primary face-centered cubic phase to hypereutectic with primary Laves phase.

https://doi.org/10.1007/s11661-019-05210-3

Multiphase alloys such as alpha-beta Ti alloys, dual-phase (DP) steels, and super alloys have delivered strength and toughness in many structural applications. The design of alloys with multiple principal elements generates the possibility of developing materials with unique properties and microstructural characteristics.[1] High-entropy alloys (HEAs) with multiphase microstructures[2] exhibit good combinations of mechanical properties. High-entropy alloys with microstructures analogous to those of DP or TRIP steels have been reported in the literature.[3] Eutectic HEAs (EHEAs) form a class of HEAs that are expected to possess good strength as well as ductility owing to their characteristic microstructure.[4,5] The good castability and strength of EHEAs have rendered them promising candidates for future high-temperature applications.[6,7] High-entropy alloys show sluggish diffusion,[8] which reduces the rate of coarsening of the eutectic microstructure. This ensures better mechanical properties due to the fine interlamellar spacing that promotes alloy strength in line with the Hall–Petch relation. The design of EHEAs with five elements is reported in the literature, and such alloys exhibit better mechanical properties than the conventional alloys do.[9–12] Different methods to determine the eutectic composition domains, including the mixing enthalpy and binary eutectic domains, have been reported.[13,14] A combination of primary phase and eutectic region confers an optimal combination of strength and ductility compared to a fully eutectic structure.[10] Proper selection of elements is required to design EHEAs with properties that can be explored for use in structural as well as high-temperature applications. The design of alloys with high-entropy phases can be explored in the EHEA domain to obtain stable microstructures. In this study, we explore a eutectic alloy with face-centered cubic (FCC) and Laves (C14 Laves) phases to provide the desired mechanical properties and stable microstructure.

High-entropy alloys with entropy stabilization can be explored if the number of elements were to be increased. A non-equiatomic alloy 35Fe10Co25Ni15Cr10V5Mn with single-phase composition with a large FCC domain was reported recently.[15] The alloy shows enhanced cryogenic as well as structural properties. In this alloy, the atomic percentage of Fe is close to the maximum concentration limit of the high-entropy domain. The eutectic alloy was designed by replacing Fe with elements that destabilize the single phase.

In this study, a eutectic alloy with seven components was designed and verified using experimental studies guided by CALPHAD tools. The eutectic alloy was designed by adding Nb to the single-phase alloy. Nb is an element that forms eutectic systems with Fe, Co, Ni, and Cr, and the eutectic composition domain was selected based on CALPHAD estimates using the TCHEA2 database from Thermo-Calc®. Figure 1(a) shows a pseudo binary-phase diagram with variation in Nb concentration plotted along the *X*-axis. The diagram shows that the eutectic point is in the range of 8 to 10 at. pct. The composition chosen for the current study is in the range of 8.66 to 9.8 at. pct Nb and is listed in Table I. The solidification pathway using Scheil's assumption (Figure 1(b)) for the hypoeutectic side (Nb = 8.66 at. pct) on the phase diagram shows the formation of the primary FCC phase followed by the formation of the eutectic region of the FCC and C14 Laves phases. Figure 1(c) shows the solidification pathway for the hypereutectic side (Nb = 9.8 at. pct) where the primary C14 Laves phase is formed from the liquid followed by the formation of the eutectic region of the FCC and C14 Laves phases. Figures 1(d) and (e) show that the FCC volume fraction is more than 70 pct with the Laves phase accounting for the remainder, which could imply better strength and ductility in these alloys. The FCC phase accounts for the ductility, and the hard Laves phase contributes to the strength. The configurational entropy of the alloy studied, as shown in Table I, confirms that the entropy of mixing increases with Nb content. We expect this increase in configurational

M.R. RAHUL and GANDHAM PHANIKUMAR are with the Department of Metallurgical and Materials Engineering, Indian Institute of Technology Madras, Chennai 600036, India. Contact e-mail: gphani@iitm.ac.in.
Manuscript submitted January 24, 2019.

Article published online April 9, 2019

Table I. Configurational Entropy Calculated Based on Composition and Experimental Results for All Compositions

Composition 10V-15Cr-5Mn-10Co-25Ni-(35-X) Fe-X Nb (Atomic Percent)	$\lvert\Delta S_{mix}\rvert$	Fraction of FCC (x) (From Experiments)	Fraction of Laves (y) (From Experiments)	$\lvert\Delta S_{mix}\rvert = (x\lvert\Delta S_{mix}\rvert_{FCC} + y\lvert\Delta S_{mix}\rvert_{Laves})$
$X = 0$	1.61R	1	0	1.61R
$X = 8.66$	1.80R	0.65	0.35	1.745R
$X = 9.5$	1.81R	0.65	0.35	1.762R
$X = 9.7$	1.815R	0.64	0.36	1.758R
$X = 9.73$	1.816R	0.49	0.51	1.760R
$X = 9.8$	1.816R	0.34	0.65	1.761R

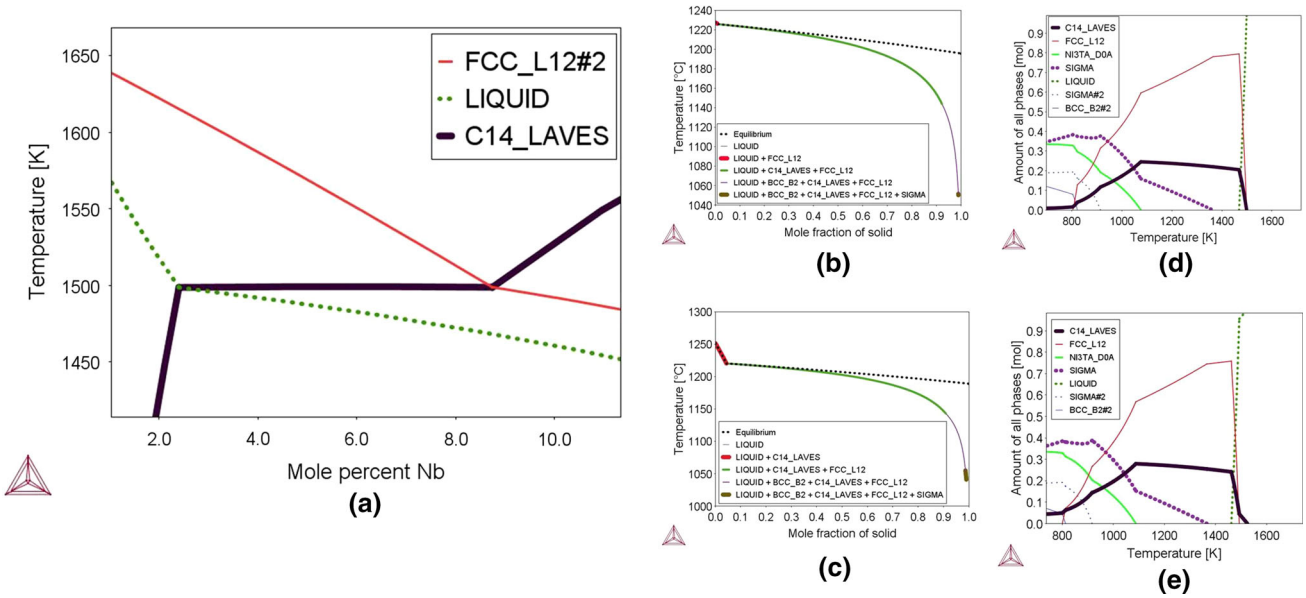

Fig. 1—(*a*) Pseudo binary-phase diagram, (*b*) Scheil's solidification pathway for $Nb_{8.66}$, (*c*) Scheil's solidification pathway for $Nb_{9.8}$, (*d*) Phase fraction with temperature diagram for $Nb_{8.66}$, (*e*) Phase fraction with temperature diagram for $Nb_{9.8}$. Alloy designations are expanded in Table I.

entropy to result in the stabilization of the microstructure for high-temperature applications.

The alloys were prepared using the technique of vacuum arc melting. The high-purity (> 99.9 pct) elements, measured in terms of atomic percentage, were placed in a vacuum chamber that was evacuated to 10^{-5} mbar. Melting was carried out using the arc created by a nonconsumable W electrode in the chamber back°filled with Ar gas. To obtain a homogeneous sample, the melting was carried out six times, with the sample being flipped at each melting. The as-cast button was suction cast to a 6-mm-diameter rod. Scanning electron microscopy (SEM) was employed to obtain backscattered electron (BSE) images of the polished samples: Quanta 400® FEG-SEM system attached with an energy dispersive spectroscopic (EDS) detector manufactured by BRUKER®was used. Compositional analysis and EDS mapping were carried out to identify the elemental partitioning between the phases. Transmission electron microscopy (TEM) was carried out on select samples using a Tecnai® instrument. The structural characterization was carried out using X-ray diffraction (XRD) (Panalytical X'pert Pro® instrument) with Cu-K_α radiation ($\lambda = 0.154056$ nm). The microhardness of each polished sample was measured using a microhardness tester with a load of 500 gf and dwell time of 10 seconds.

The BSE-SEM images of the as-cast samples are displayed in Figures 2(a) through (e), showing that change in Nb concentration affects the formation of the eutectic region. The solidification pathways as well as the morphologies of the phases formed differed at hypereutectic and hypoeutectic concentrations. In the case of $Nb_{8.66}$ and $Nb_{9.5}$ alloys, the solidification pathway can be expressed as Liquid → Liquid + FCC, followed by Liquid → Laves phase + FCC (eutectic reaction). Table II shows the compositions of the individual phases, and reveals that the primary FCC phase is rich in Cr and Fe. The Laves phase is enriched with Nb. Co is distributed almost equally between the phases. The individual configuration entropies of the different phases, as shown in Table II, confirm that the elements chosen in the system yield high-entropy phases. The configurational entropies calculated based on phase fractions are shown in Table I, and all the values are greater than 1.5R, which qualifies the alloy in the

Table II. Compositions of Individual Phases Measured by EDS Point Analysis and Calculated Configurational Entropy Based on EDS Composition

FCC Phase								
10V-15Cr-5Mn-10Co-25Ni-(35-*X*) Fe-*X* Nb (Atomic Percent)	Fe	Ni	Cr	V	Co	Mn	Nb	$\lvert\Delta S_{mix}\rvert_{FCC}$
X = 8.66	31.41	25.10	15.66	10.62	10.47	4.31	2.44	1.70R
X = 9.5	30.04	25.20	16.50	10.56	10.39	4.97	2.56	1.72R
X = 9.7	29.45	25.37	16.35	10.60	10.29	4.85	3.10	1.73R
X = 9.73	28.37	26.69	15.95	11.07	9.98	5.01	2.64	1.72R
X = 9.8	28.19	26.34	15.80	11.03	10.16	5.10	3.37	1.74R
Laves Phase								
10V-15Cr-5Mn-10Co-25Ni-(35-*X*) Fe-*X* Nb (Atomic Percent)	Fe	Ni	Cr	V	Co	Mn	Nb	$\lvert\Delta S_{mix}\rvert_{Laves}$
X = 8.66	24.12	22.89	13.07	9.78	10.58	4.35	15.22	1.83R
X = 9.5	24.15	22.69	14.47	9.87	10.49	4.32	14.01	1.84R
X = 9.7	27.41	18.83	15.51	7.70	10.96	4.02	15.56	1.81R
X = 9.73	26.49	17.95	13.79	6.40	11.17	3.69	20.51	1.80R
X = 9.8	26.44	18.04	13.95	6.21	11.46	3.66	20.25	1.80R

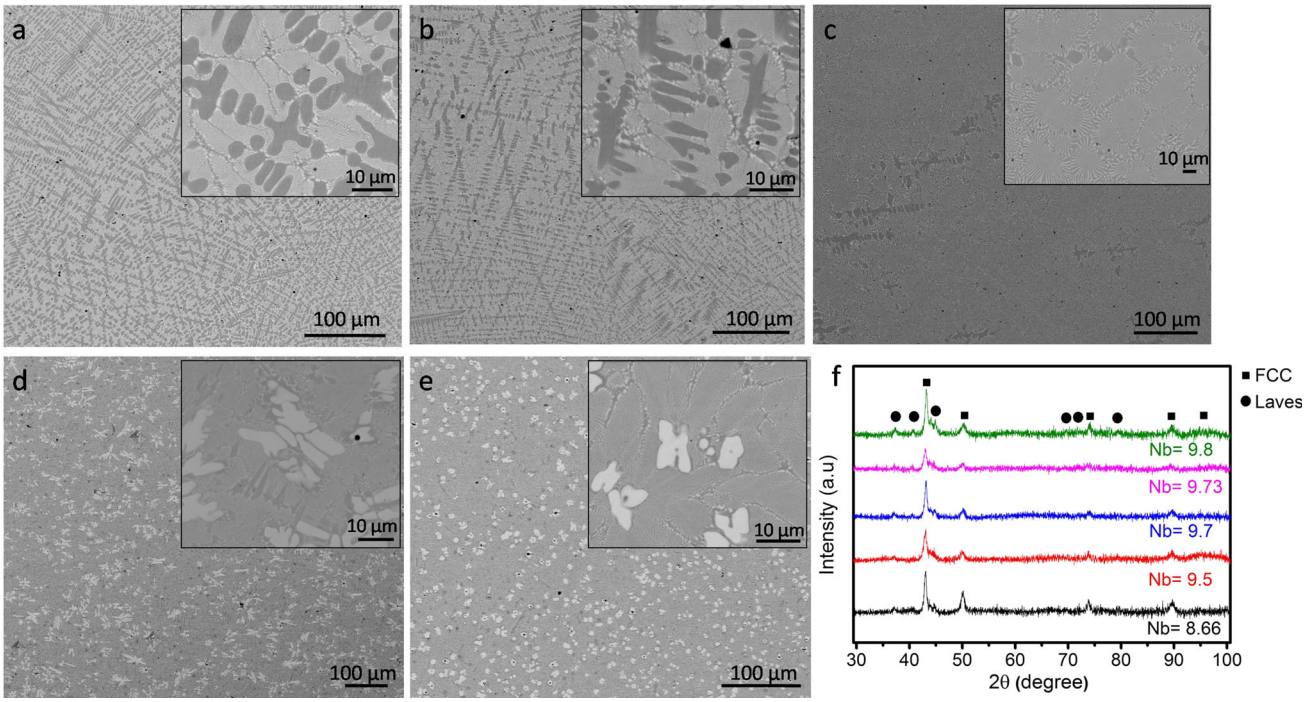

Fig. 2—SEM-BSE images for alloys (*a*) $Nb_{8.66}$, (*b*) $Nb_{9.5}$, (*c*) $Nb_{9.7}$, (*d*) $Nb_{9.73}$, (*e*) $Nb_{9.8}$, (*f*) XRD pattern for all composition. Alloy designations are expanded in Table I.

two-phase solid state to be referred to as a HEA. An important feature of this alloy is that the difference in the elements segregated across the two phases renders the diffusion processes sluggish and promotes stability of the microstructure. The XRD patterns confirm the presence of the Laves phase (Nb-rich, with hexagonal close-packed (HCP) structure, C14 Laves phase) and FCC phase (rich in Fe, Cr) in the alloy.

Figure 2(c) shows the $Nb_{9.7}$ condition that has the highest eutectic fraction as well as the smaller interlamellar spacing among all the samples. The solidification pathway is similar to that of the $Nb_{8.66}$ condition as is the elemental partitioning, as shown in Table II. The pro-eutectic FCC phase shows a dendritic morphology with the interdendritic region enriched with the eutectic. The hypereutectic region is seen in the $Nb_{9.73}$ and $Nb_{9.8}$ compositions wherein the solidification pathway is as follows: Liquid → Liquid + Laves phase, followed by Liquid → Laves phase + FCC (eutectic reaction). The EDS mapping (Figure S2) shows the

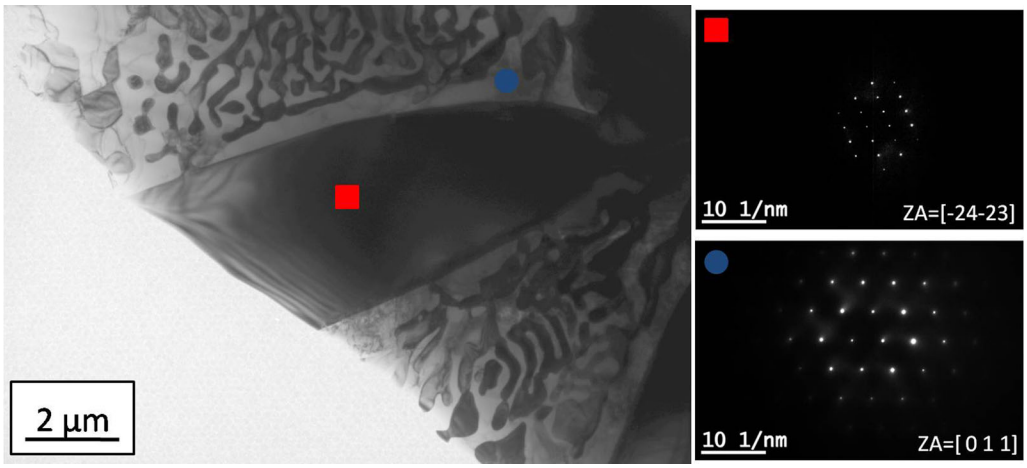

Fig. 3—TEM micrograph of $Nb_{9.73}$ alloy.

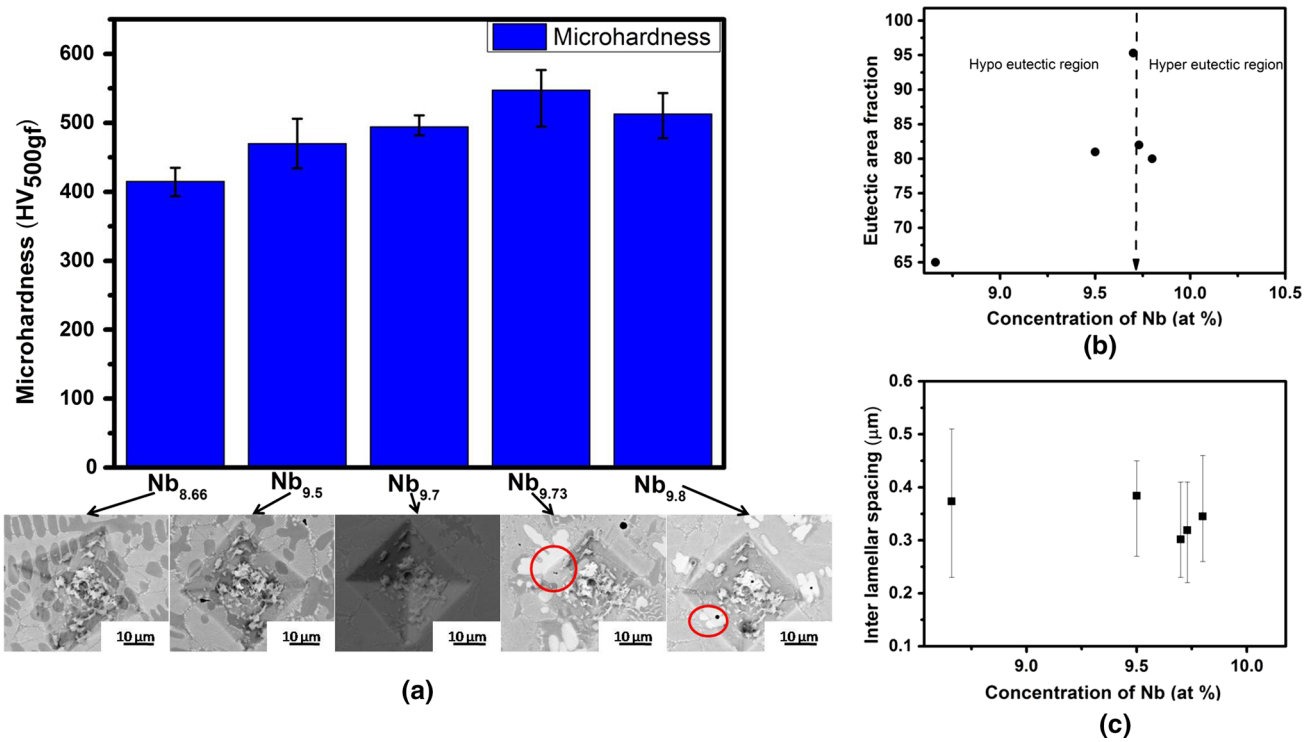

Fig. 4—(*a*) Variation of microhardness with respect to Nb concentration; (*b*) variation of eutectic area fraction with respect to Nb concentration; (*c*) variation of interlamellar spacing with respect to Nb content.

depletion of Fe, Cr, Ni, V, and Mn from the primary Laves phase, but their concentrations remain in the high-entropy domain. The morphology of the Laves phase is different than that of the primary FCC phase in the hypoeutectic condition. The $Nb_{9.8}$ condition shows a branched morphology for the primary Laves phase with a sixfold symmetry that can be attributed to the HCP structure of the C14 Laves phase. Figure 2(f) shows the XRD pattern that confirms the formation of the FCC and Laves phases at all compositions. The peak intensity varies with phase fraction. The inset in the images (Figures 2(a) through (e)) shows the eutectic microstructure with lamellar morphology at a higher magnification. The composite microstructure obtained by varying the Nb and Fe contents provides the compositional window to explore improved mechanical properties. The

microstructures reveal that the fully eutectic point lies in the Nb concentration range 9.7–9.73 at. pct.

Figure 3 shows the TEM image of the $Nb_{9.73}$ condition wherein the primary Laves phase and eutectic region are present. The diffraction pattern confirms that the primary phase is the C14 Laves phase with a HCP lattice and the eutectic consists of the FCC and Laves phases. The TEM and XRD studies confirm the applicability of the CALPHAD approach in guiding the design of specific alloys. The predictions match with the experimental results and enable the identification of an optimal composition of this seven-component alloy system.

The microstructure is correlated with the microhardness measurements. Figure 4(a) shows the variation in microhardness with the increasing Nb content. It was found that the microhardness increases with the Nb content as the latter increases up to 9.73 at. pct, and decreases thereafter. Both the primary phase and the eutectic region contribute to the microhardness changes measured. The SEM images of indentation reveal contributions from both the regions. The hardness is in the range of 400 to 600 HV, which is comparable to those of $CoCrNiFeNb_x$ alloys.[9] The $Nb_{9.7}$ condition shows the hardness of the eutectic region wherein the indentation is completely concentrated on the eutectic region, and the average value of hardness is 500 HV. Figures 4(b) and (c) show the eutectic area fraction and interlamellar spacing. The eutectic area fraction increases with Nb content in the hypoeutectic region and decreases in the hypereutectic region. This can be attributed to the partitioning of Nb in the primary phase in the hypereutectic condition. It is found that hardness is higher in the hypereutectic region than in the hypoeutectic region, and this can be attributed the strengthening effect offered by the primary Laves phase in the hypereutectic region. The hard and brittle Laves phase ensures high hardness, as can be seen from the cracks forming in the indented region (highlighted with red circles in the SEM image in Figure 4(a)). The interlamellar spacing decreases with the increasing Nb content, and this also causes the increase in hardness in the hypoeutectic region, as expected from the Hall–Petch relation. In the hypereutectic region, the interlamellar spacing increases with the increasing Nb content.

A new EHEA with seven components ((35-x)Fe-10Co-25Ni-15Cr-10V-5Mn-xNb) was designed using an optimal combination of experiments guided by CALPHAD estimates. The solidification pathway was confirmed and correlated well with the microstructure's formation. The eutectic is formed between the Nb-rich Laves phase with HCP structure and the FCC phase. The variation in microhardness correlated well with the interlamellar spacing and eutectic fraction.

M.R. Rahul would like to acknowledge B. Nithin, Shah Naishalkumar Sanjay, and Sumanta Samal for useful discussions.

ELECTRONIC SUPPLEMENTARY MATERIAL

The online version of this article (https://doi.org/10.1007/s11661-019-05210-3) contains supplementary material, which is available to authorized users.

REFERENCES

1. D.B. Miracle and O.N. Senkov: *Acta Mater.*, 2016, vol. 122, pp. 448–511.
2. W.H. Liu, Z.P. Lu, J.Y. He, J.H. Luan, Z.J. Wang, B. Liu, Y. Liu, M.W. Chen, and C.T. Liu: *Acta Mater.*, 2016, vol. 116, pp. 332–42.
3. Z. Li, K.G. Pradeep, Y. Deng, D. Raabe, and C.C. Tasan: *Nature*, 2016, vol. 534, pp. 227–30.
4. S. Samal, M.R. Rahul, R.S. Kottada, and G. Phanikumar: *Mater. Sci. Eng. A*, 2016, vol. 664, pp. 227–35.
5. M.R. Rahul, S. Samal, S. Venugopal, and G. Phanikumar: *J. Alloys Compd.*, 2018, vol. 749, pp. 1115–27.
6. L. Yiping, Y. Dong, S. Guo, L. Jiang, H. Kang, T. Wang, B. Wen, Z. Wang, J. Jie, Z. Cao, H. Ruan, and T. Li: *Sci. Rep.*, 2014, vol. 4, p. 6200.
7. L. Yiping, X. Gao, L. Jiang, Z. Chen, T. Wang, J. Jie, H. Kang, Y. Zhang, S. Guo, H. Ruan, Y. Zhao, Z. Cao, and T. Li: *Acta Mater.*, 2017, vol. 124, pp. 143–50.
8. K.-Y. Tsai, M.-H. Tsai, and J.-W. Yeh: *Acta Mater.*, 2013, vol. 61, pp. 4887–97.
9. F. He, Z. Wang, P. Cheng, Q. Wang, J. Li, Y. Dang, J. Wang C.T. Liu: *J. Alloys Compd.*, 2016, vol. 656, pp. 284–89.
10. W. Huo, H. Zhou, F. Fang, Z. Xie, and J. Jiang: *Mater. Des.*, 2017, vol. 134, pp. 226–33.
11. F. He, Z. Wang, S. Niu, W. Qingfeng, J. Li, J. Wang C.T. Liu Y. Dang : *J. Alloys Compd.*, 2016, vol. 667, pp. 53–57.
12. M. Zhang, L. Zhang, P.K. Liaw, G. Li, and R. Liu: *J. Mater. Res.*, 2018, vol. 33, pp. 3276–86.
13. L. Yiping, H. Jiang, S. Guo, T. Wang, Z. Cao, and T. Li: *Intermetallics*, 2017, vol. 91, pp. 124–28.
14. H. Jiang, K. Han, X. Gao, L. Yiping, Z. Cao, M.C. Gao, J.A. Hawk, and T. Li: *Mater. Des.*, 2018, vol. 142, pp. 101–105.
15. Y.H. Jo, S. Jung, W.M. Choi, S.S. Sohn, H.S. Kim, B.J. Lee, N.J. Kim, and S. Lee: *Nat. Commun.*, 2017, vol. 8, pp. 1–8.